752 *KSME International Journal, Vol. 13, No. 10, pp. 752~761, 1999*

Acoustic Scaling of an Axial Fan with Non-Uniform Inlet Flows

Seungbae Lee* and Gwi-Chul Yang**

(Received December 28, 1998)

An experimental study was carried out to vary circumferential and radial components of incoming disturbances for a propeller-type axial fan connected to an anechoically terminated inlet duct. It was suggested that the acoustic pressure from rotating blades encountering a low-frequent gust have the scaling parameter of $\rho_0 c_0 |\underline{a}| Ma$, while the one for a high-frequent gust be properly scaled by $\rho_0 c_0 |\underline{a}|$. Here $\rho_0 c_0$, $|\underline{a}|$, Ma are the characteristic impedance of medium, the amplitude of disturbed velocity, and Mach number, respectively. These scalings were applied to identify both compact and non-compact noise sources from low-frequent gusts using the spectral decomposition method. The method of acoustic scaling proposed in this study turned out to be more effective for the sound radiated into a duct by the interaction of low-frequent incoming gusts with the propeller fan than previous approaches.

Key Words: Propeller-Type Axial Fan, Noise, Acoustic Scaling, Spectral Decomposition

1. Introduction

This paper is concerned with noise generated by an axial fan with non-uniform inlet flows. The propeller-type axial fans have been increasingly utilized in home appliances for the convective cooling, e. g. in air-conditioning units. The non-uniform inlet flows by unavoidable obstacles located upstream often generate increased tonal noise.

Recently, the spatial compactness becomes inherent with the growing width of application of the propeller-type axial fan. Consequently, non-uniform flows are frequently encountered at a blade inlet and result in a significant increase in the discrete frequency sound level. This type of unsteady lifting surface problem is known as a gust problem in marine/aerodynamic applications or called as an inlet distortion in turbomachines. The problem of propeller-gust interaction has been treated recently by a semi-analytical method (Attasi et al., 1990).

The "Fan Sound Law" attempted by Madison in 1949 has been the subject of considerable speculation and controversy. The tip speed exponent for the sound power ranges from 4.6 to 6.0 even for the discrete frequency sound. Weidemann (1971) decomposed the radiated sound from the uncased centrifugal impellers with a rectangular wedge into a normalized spectral distribution function and an acoustic frequency response function. Following Weidemann's formulation of the similarity law, Neise (1975) performed a similar experiment for the two dimensionally similar centrifugal fans with identical impellers to those of Weidemann. He measured a value of 4.6 different from 5.6 by Weidemann for the impeller tip speed exponent of sound power. The discrepancy in the U-dependence of sound law was also observed by Longhouse (1976), who examined the rotational noise for the inflow distortion and turbulence by installing the circular rods upstream for a low tip-speed axial fan. He explained the discrepancy by the reason that the inflow distortion and turbulence may not increase in direct proportional to the tip speed. Margetts (1987) demonstrated that the equivalent acoustic source from an axial fan is of a dipole

* Department of Mechanical Engineering, INHA University, 253 Yonghyun-dong, Nam-gu, Incheon 402-751, KOREA

** Graduate Student, Flow Noise Control Laboratory, INHA University, Incheon 402-751, KOREA

nature from the measurement of phases from inlet and outlet noise. But his elaborate measurement of dipole source does not explain the departure of a speed scaling index over a range of speeds and with a range of duct lengths.

The idea of discrete source identification in turbomachinery using the spectral decomposition method was extended by Mongeau et al. (1993) to investigate the relatively low frequency aerodynamic source of rotating stall and broadband noise sources. The dynamic pressure, ρV_{tip}^2, and the rotational time of D/V_{tip} were used to scale the acoustic pressure and the characteristic time of acoustic correlation in their spectral decomposition method. It did not include the effect of acoustic impedance upon radiation from impellers installed in the duct. Their effects were naturally thrown into the source spectral distribution function, which is not supposed to affect sound radiation efficiency.

As was discussed by Neise(1975), there might be no hope for finding a universal value for the impeller tip speed exponent. But the source identification methods, which can be implemented with ease, are now sought and the spectral decomposition method is one of the candidates for assessing fan noise source characteristics. For this purpose, the scaling parameters of an acoustic pressure spectral density function need to be re-examined on the physical ground of order of magnitude analysis for non-uniform incoming flows. In the present work, flow conditioners designed to introduce non-uniformity to the flow were installed in an acoustically lined duct. Experiments were conducted using a propeller-type axial fan discharging directly into the atmosphere in order to investigate the noise source characteristics for non-uniform inlet flows. The objective of this study is to develop acoustic scaling parameters for inflow distortions of low-frequent gusts and identify each noise source characteristics for various non-uniform inlet conditions.

2. Mathematical Background of Scaling Parameters

There are two approaches to the study of aeroacoustics (Goldstein, 1976): one is to directly solve a set of linearized governing equations specifically for sound generation due to the pressure fluctuations on a solid boundary in a moving medium, the other is to follow the Lighthill's acoustic analogy(1952) deduced from governing equations. Based on Lighthill's theory, Ffowcs Williams and Hawkings(1969) have established a more general aeroacoustic theory for a moving solid boundary in a non-stationary medium. Here we follow the Goldstein's approach to scale the noise generated by the rotating fan blades.

The non-uniform inlet flow of approaching gusts to a rotating blade can be classified into a high-frequent gust problem and low-frequent one depending on a characteristic time-scale involved. If the characteristic time-scale of harmonic disturbance of incoming gusts in the blade frame of reference is of comparable magnitude with an acoustic time-scale, this may be called as a high-frequent gust problem. The low-frequent gust problem specifies that the characteristic time-scale involved in the noise generation is longer than the acoustic traveling time-scale as shown in Table 1.

Table 1 Classifications using terminologies in this study for non-uniform inlet flows and non-uniform inflow turbulence noise.

Non-uniform inlet flow of incoming gust	High-frequent gust	$(p_\theta\Omega_0)^{-1}$(gust frequency^{-1}) $\sim r_o/c_o$(acoustic time-scale)
	Low-frequent gust	$(p_\theta\Omega_0)^{-1} \gg r_o/c_o$(acoustic time-scale)
Non-uniform inflow turbulence noise	Compact source (low frequency noise)	Λ(size of eddy) $\gg$ C(blade chord length)
	Non-compact source (high frequency noise)	Λ(size of eddy) $\ll$ C(blade chord length)

The non-uniform inflow-turbulence noise can be classified into low-frequency and high frequency inflow noise, depending on whether the length of disturbance is longer than the blade chord or not. If the size of eddy is much bigger than the chord of blade, the blade will experience a fluctuation of total lift as a whole. This situation occurs in the atmospheric turbulence noise from the wind turbine causing sound radiation of Ma^6 because the blade can be regarded to be acoustically compact. In the other case of small-sized eddy comparable or less than the dimension of blade, the blade will respond only locally and radiate sound scattered at the leading and trailing edges varying with Ma^5(Ffowcs Williams et al., 1970). The present paper is concerned with the effects of both non-compact sources of high frequency and compact sources of low-frequency inflow turbulence upon radiated sound for the low-frequent gust problem.

The aerodynamics at each radial station can be applied to thin strips of a blade as shown in Fig. 1. This figure shows an aerodynamic transformation from the inertial frame of reference with the x_1 axis aligned with the mean inflow to the blade frame of reference.

In order to obtain the first order estimate of scaling parameters, the upstream distortion is given in cylindrical polar coordinates in terms of the circumferential and radial harmonics.

$$\underline{V}_\infty(\underline{x}) = V_\infty \underline{i}_1 + \underline{a}\cdot e^{-i\left(\frac{2\pi}{\lambda_r}r + p_\theta \theta\right)} \tag{1}$$

where $p_r = (r_t - r_h)/\lambda_r$ (λ_r : the radial wavelength of disturbance, r_t, r_h : tip and hub radii of fan) and p_θ is an integer for azimuthal disturbance. The upstream flow in the blade frame of reference becomes

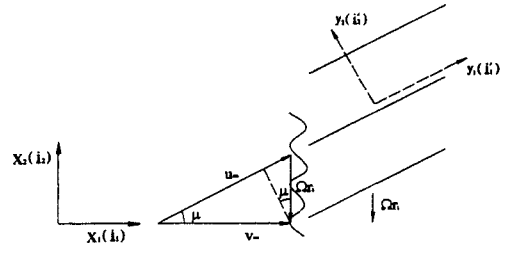

Fig. 1 Aerodynamic transformation of coordinates.

$$\underline{u}_\infty(\underline{y}, t) = u_\infty \underline{i}_1' + \underline{a}\cdot e^{i(\omega t - \underline{k}'\cdot\underline{y}')} \tag{2}$$

where k_1', k_2', and k_3' are the wave numbers in the blade frame of reference. The details can be found in Attasi et al. (1990). The total velocity in the rotationg frame can then be written as

$$\underline{u}(\underline{y}, t) = u_\infty \underline{i}_1' + \underline{a}\cdot e^{i(\omega' t - \underline{k}'\cdot\underline{y}')} + \underline{u}_a(\underline{y}, t) \tag{3}$$

where $\underline{u}_a(\underline{y}, t)$ is the flow disturbance of acoustic potential part which results from the interaction of $\underline{a}\cdot e^{i(\omega t - \underline{k}'\cdot\underline{y}')}$ with blade. The far-field of $\underline{u}_a(\underline{y},t)$ represents the sound radiated from the blade. From the linearized Euler equations for $\underline{u}_a(\underline{y}, t)$, we get

$$\frac{D_o}{Dt}\rho' + \nabla\cdot\underline{u}_a = 0 \tag{4}$$

$$\rho_o\left(\frac{D_o}{Dt}\underline{u}_a + 2\underline{\Omega}\times\underline{a}\cdot e^{i(\omega' t - \underline{k}'\cdot\underline{y}')} + 2\underline{\Omega}\times\underline{u}_a\right) + \text{higher order terms} = \nabla p' \tag{5}$$

where $\frac{D_o}{Dt} = \frac{\partial}{\partial t} + u_\infty \frac{\partial}{\partial y_1'}$.

We normalize the length with respect to the fan radius (r_o) and the velocity with respect to the amplitude of disturbance velocity and use a rotating time scale of Ω_o^{-1} where Ω_o is the angular velocity of rotating blade. The last two terms on left-hand side of Eq. (5) come from the Coriolis motion in the rotating coordinate system. It is convenient to express p' in a series of Mach number in an ascending order as

$$p' = \rho_o r_o \Omega_o |\underline{a}| (\overline{P}_o' + Ma\cdot\overline{P}_1' + Ma^2\cdot\overline{P}_2' + \cdots) \tag{6}$$

where $Ma = r_o\Omega_o/c_o$ and c_o is the speed of sound. Substituting Eq. (6) into Eq. (5) and normalizing the linearized momentum equation, the non-dimensional equation in a leading order (Ma^0) can be written as follows:

$$\frac{D_o}{Dt}\overline{u}_a + 2\overline{\Omega}\times\overline{u}_a + 2\underline{\Omega}\times\underline{a}\cdot e^{i(\overline{\omega}'\overline{t} - \underline{\overline{k}}'\cdot\underline{\overline{y}}')} = -\nabla\overline{P}_0' \tag{7}$$

where overlined quantities mean to be normalized. The unsteady pressure, which will be used to get an acoustic auto-correlation, is shown to have the leading order of $\rho_o c_o |\underline{a}| Ma = (\rho_o r_o \Omega_o |\underline{a}|)$ for the low-frequent gust problem.

For the high-frequent gust, a characteristic time scale of acoustic travelling time ($=r_o/c_o$) is

suggested intuitively for normalization. Normalizing Eq. (5) with this scaling gives the acoustic pressure of $\rho_0 c_0 |\underline{a}|$ as a leading order term in the blade frame of reference. Therefore the irrotational motion of $\underline{u}_a$ degenerates into an acoustic wave equation in the leading order in this case.

While the acoustic pressure can be scaled by $\rho_0 V_{tip}^2$ for the low-frequent gust problem, the quantity of $\rho_0 c_0 V_{tip}$ can be used to scale acoustic pressure for the high-frequent one, assuming that the amplitude of the rotational motion due to an incoming gust increases linearly with the rotational speed of fan.

3. Experimental Procedure

An experimental device, shown schematically in Fig. 2 was installed in an anechoic chamber of Flow Noise Control Laboratory at INHA University. The propeller-type axial fan tested has a diameter of 400mm and 3 blades. The principal physical characteristics are listed below.

Table 2 Physical properties of the axial-type propeller fan.

Physical Characteristics	
Diameter (mm)	400
Hub to Tip Diameter Ratio	0.29
Nominal Fan Speed (rev/min)	800
Flow-rate Coefficient at Design Point	0.43
Pressure Coefficient at Design Point	1.33
Chord Length (mm)	64 (hub) ~ 292 (tip)
Solidity	0.611 ~ 0.697

International standard ISO 5136 specifies an engineering method to determine the sound power level using an in-duct configuration. For an installation type of ducted inlet and free outlet, the test section of the circular duct must have a length greater than 6 times the duct diameter and be connected to an anechoic termination, satisfying specified maximum pressure reflection coefficients for the frequency range between 100Hz and 10,000Hz. The duct used in this work is acoustically lined with glass wools having a density of 45kg/m^3, 60% open, and of circular cross-section without any transition. The frequency range of interest lies between 50Hz and 550Hz to cover the first eight BPF components. Only plane wave propagates in a rigid wall if the frequency is small enough that

$$f < \frac{\pi c_0}{1.84D}(1-Ma^2)^{\frac{1}{2}} \cong 1380\text{Hz} \qquad (8)$$

The acoustically lined duct also eliminates the problem of radial standing mode in the test duct at the low frequency range of interests.

The duct used in this study introduces very uniform flow with low turbulence levels to the rotating blades by using the combination of honey-comb and two screens of 32-mesh size. An anechoic termination is installed upstream of the test section to minimize the effect of an axial standing wave and to provide an acoustic loading

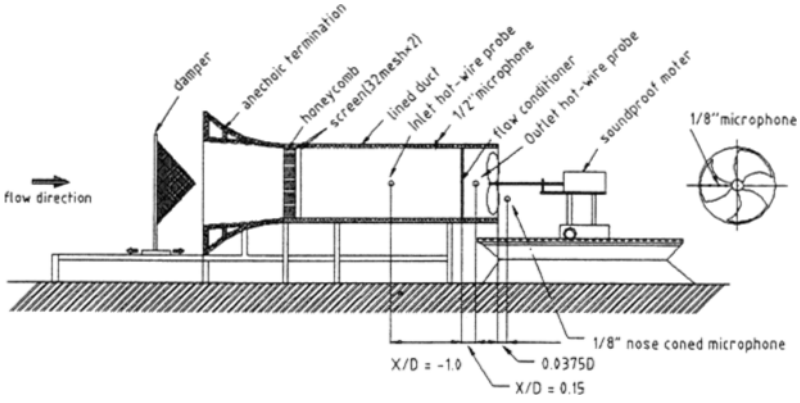

Fig. 2 Schematic of in-duct measurement set-up with flow conditioner and anechoic termination.

on the blades nearly equal to the characteristic impedance of the air. The test duct of a short length also makes the growth of a boundary layer to be confined, which is important to generating specified non-uniform inlet flows. When the Reynolds number based on the duct diameter is about 10^5, the entrance length is about 30 times of that which is comparable with the length of the test duct for a standard in-duct method. Therefore it is desirable for this purpose to have a test duct of a short length unless resonance may occur.

Upstream of the propeller fan is located a flow conditioner designed to generate circumferential and radial components of non-uniform incoming flow. Figure 3 shows the slotted flow conditioners for the azimuthal and radial disturbances. The mechanical apparatus driving the propeller fan consists of a shaft, a bearing assembly and an adapter. A one kilowatt D. C. motor is controlled to vary the shaft rotational speed and covered by 5mm thick steel wall with glass wools filled inside. The shaft speed of the motor is measured using an encoder device sending 3600 pulses per one revolution. A microphone of Brüel & Kjær 1/2″ size is mounted flush with the inlet duct wall and a B&K 1/8″ pressure-type microphone with a nose-cone is located just downstream of the propeller fan for the cross-spectrum measurements. To measure the distributions of mean axial velocity and turbulent intensity downstream of the flow conditioner, an I-type hot-wire sensor is traversed across the duct cross-section.

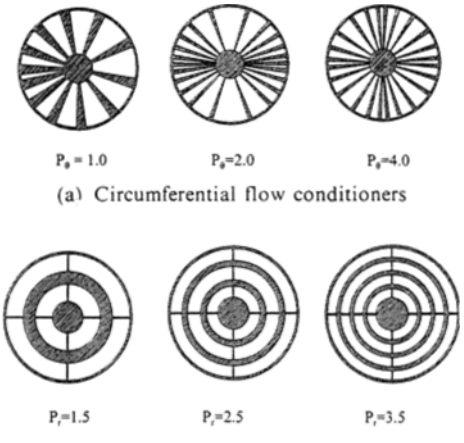

Fig. 3 Flow conditioners designed to generate non-uniform inflows(shaded region for blockage).

4. Measured Spectra and Spectral Decomposition

The aerodynamic performance of the propeller fan is first measured by following the standard by ANSI/AMCA210-85. The non-dimensional pressure coefficients ($\Psi=\Delta p/(\rho N^2D^2)$) for the propeller fan tested are drawn with respect to the non-dimensional flow-rate ($\phi=Q/(ND^3)$) in Fig. 4. The units used in non-dimensional parameters are m^3/sec, rev/s, meter, Pascal, kg/m^3 for Q, N, D, Δp, and ρ, respectively.

The flow conditioner is located at a short distance (0.15D) upstream of the fan. Figure 5 shows the measured mean axial velocity distributions for radially slotted flow conditioners. The loading conditions are set to have a flow coefficient close to 0.35 regardless of the type of flow

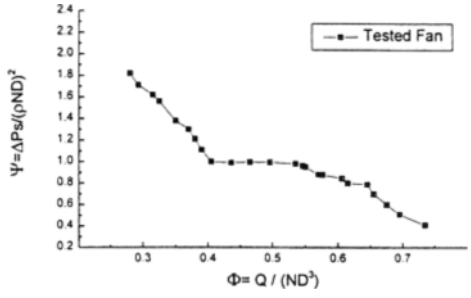

Fig. 4 Performance curve of propeller fan employed.

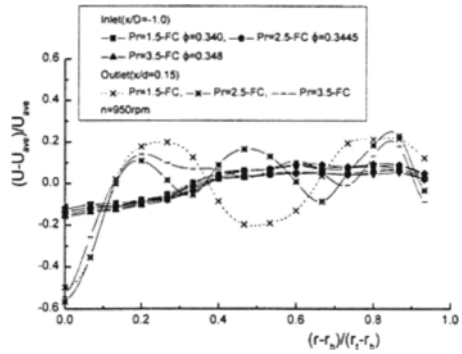

Fig. 5 Distributions of velocity for three radial flow conditioners.

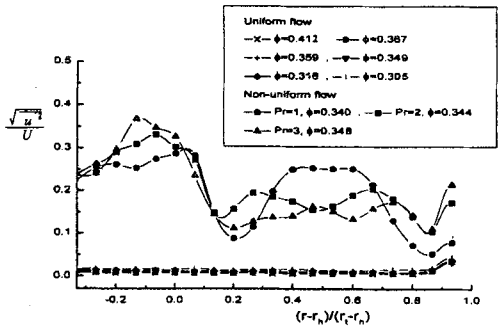

Fig. 6 Distributions of turblulence intensity for radial flow conditioners.

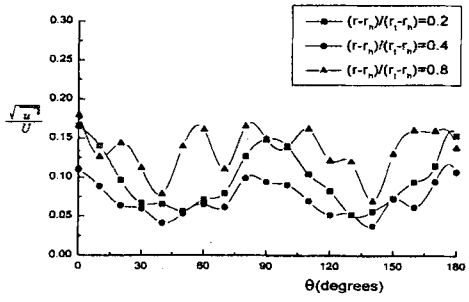

(a) The case of $p_\theta=2$

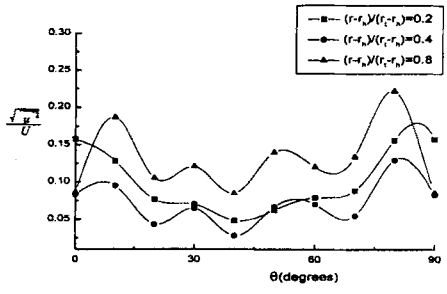

(b) The case of $p_\theta=4$

Fig. 7 Distributions of turbulence intensity for flow conditioners of $p_\theta=2,4$.

conditioner by adjusting a damper. This flow coefficient corresponds to the relatively unstable region where the primary mode of downstream flow changes from a radial flow to an axial flow. This kind of instability was reported for a small, low tip speed, and ducted axial fan by Krane et al. (1993). Choi(1994) also found an instability mode of harmonically related broad humps at low frequency in a centrifugal impeller without diffuser and casing.

The disturbances from the first two radial flow conditioners in Fig. 3(b) are observed to have the wave lengths of $2/3(r_t-r_h)$ and $2/5(r_t-r_h)$ approximately, reflecting $P_r=1.5$ and 2.5, respectively. The averages of turbulence intensities over cross-section area are increased from 1% to 17%~18% by placing the flow conditioners upstream of the fan. The turbulence intensity upstream of the fan for the flow conditioner of $P_r=1.5$, as shown in Fig. 6, has a rapid increase near the hub, which may be considered to radiate non-BPF sound by a rotating instability. The flow conditioners for the azimuthal disturbances do not introduce so uniform in the radial direction as what is intended and the case of $p_\theta=2$ represents the non-consistent variations of turbulent intensity compared with the case of $p_\theta=4$, as shown in Fig. 7. It can be deduced that the case of $p_\theta=2$ would have less contributions to the tonal sound energy than the other cases of $p_\theta=1$ and 4.

Table 3 Sound power indices of rotational speeds for the cases of non-uniform inflow condition.

	ϕ	T.I. (Averaged Turbulence Intensity)	Sound power slope(m)
$P_r=1.5$	0.340	0.171	4.5
$P_r=2.5$	0.344	0.182	4.9
$P_r=3.5$	0.348	0.169	5.1
$P_\theta=1$	0.362	0.165	5.5
$P_\theta=2$	0.340	0.184	5.0
$P_\theta=4$	0.343	0.140	5.1

The sound powers are measured using a 1/2″ microphone flush-mounted on the duct. According to Neise(1995), in the frequency range of higher-order mode sound propagation, the in-duct sound power levels were lower than the free-field sound power levels. Table 3 gives the measured sound power indices of the rotational speed for each case of non-uniform inflow conditions. The scaling indices around 5.0 are measured for the radial disturbances, which have high turbulence intensity levels. This may be explained by the fact that the local pressure fluctuations on the impeller from the incoming turbulent eddies radi-

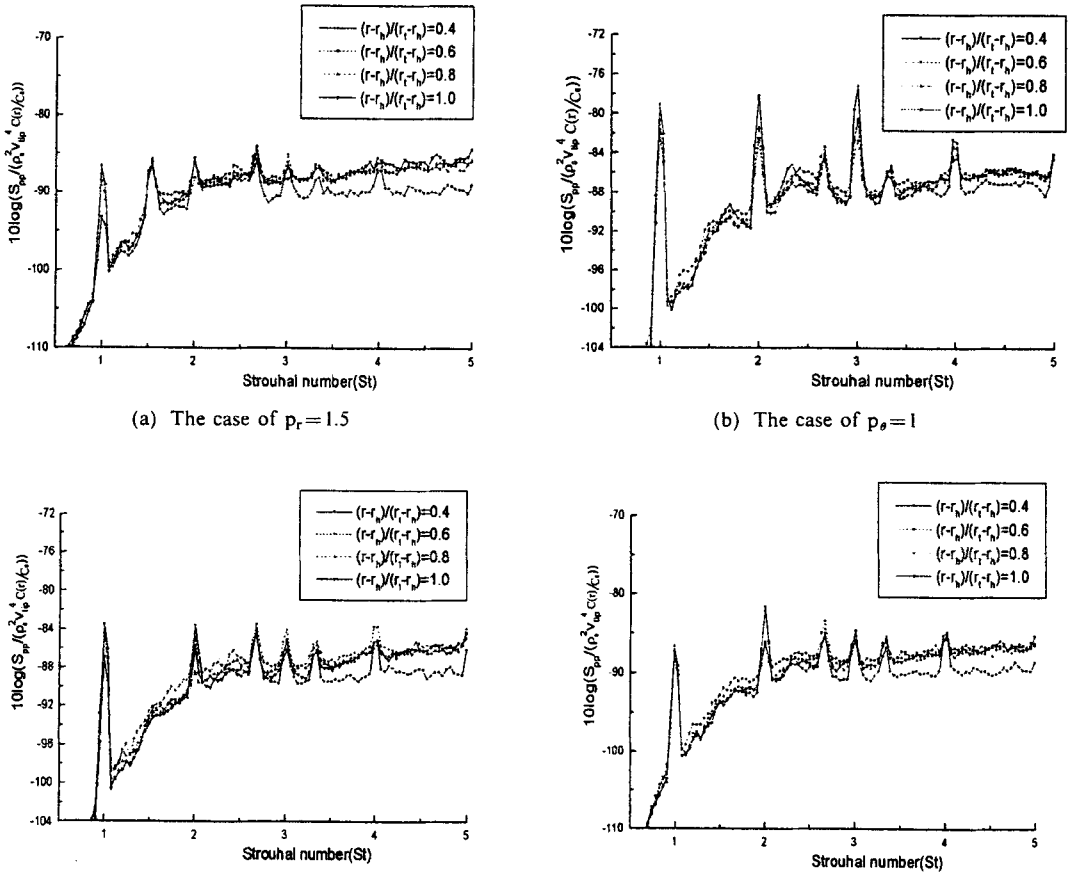

(a) The case of $p_r=1.5$

(b) The case of $p_\theta=1$

(c) The case of $p_\theta=2$

(d) The case of $p_\theta=4$

Fig. 8 Normalized cross-spectra between near-field pressure and acoustic pressure from flush-mounted microphone with inlet duct.

ate non-compact sound. The periodic changes in the angle of attack from azimuthal variations of incoming gusts make the sound scaling index to be increased up to 5.5 for the case of $p_\theta=1$. The cases of p_θ equal to 2 and 4 show similar results to the radial disturbances by the reason that the wave length, Λ, of disturbances is short enough to have non-compact radiations. The cases of P_r equal to 1.5 has a relatively low index with the instability mode at a Strouhal number of 1.54, though having a high turbulance intensity, which can be seen in its source spectral distribution function.

A 1/8″ nose-coned pressure type microphone (B&K4138 model) is placed near 0.0375D downstream of the trailing edge and traversed radially to measure the cross-spectra together with the pressure from a flush-mounted microphone inside the duct. The non-dimensional sound pressure cross-spectral density $S^*_{PP'}$ is expressed in the form:

$$S^*_{pp'}(f)=\frac{S_{pp'}(f)}{(\rho_0 V^2_{tip})^2\cdot(C(r)/c_0)} \tag{9}$$

where the acoustic pressure and the frequency were normalized by $\rho_0 V^2_{tip}$ and $C(r)/c_0$ ($C(r)$; chord length) at each radial station, respectively. Figure 8 shows typical results from normalized cross-spectra taken at a few radial stations for the cases of $p_r=1.5$ and $p_\theta=1.0$, 2.0, and 4.0. The sound pressure cross-spectral density is compared with the auto-spectral density S_{pp}, which is measured from the microphone flush-mounted with the inlet duct.

The non-dimensional radiated sound pressure auto-spectral density can be expressed as the product of an acoustic system response function G and a source spectral distribution function F:

$$\frac{\sqrt{S_{pp}(f)}}{\rho_0 V_{tip}^2 \sqrt{D/c_0}} = G(He, \phi) \cdot F(St, \phi) \quad (10)$$

where $He = fD/c_o$, $St = \pi fD/(V_{tip} \cdot n)$, and n is the number of blade. The Helmholtz number, He, characterized by the ratio of the fan diameter and the acoustic wave length, explains acoustic phenomena such as resonance and sound reflection. The Strouhal number, St, is defined as the ratio of the sound frequency and the blade passage frequency. The pressure magnitude in the spectral density S_{pp} is scaled by $\rho_0 V_{tip}^2$ with the assumption that incoming turbulent intensity remains constant because the inverse of gust frequency, $(p_\theta \Omega_0)^{-1}$, is greater than the acoustic time-scale, r_0/c_0, for all the cases considered in our study. The characteristic time used in the integration of S_{pp} may be either an acoustic travelling time or an aerodynamic convective time. The sound pressure auto-spectral density of $S_{pp}(f)$ is normalized by either $\rho_0^2 V_{tip}^4 (D/c_0)$ or $\rho_0^2 V_{tip}^3 D$, depending on the time-scale used in the correlation, both of which are employed in this study to identify noise sources.

Keeping ϕ and x/D fixed and taking logarithm on both sides of Eq. (10), the acoustic system response function can be re-written as

$$20 \log G(He) = L_{pp}(f, V_{tip}) - 40 \log V_{tip} - 10 \log (\rho_0^2 D \Delta f_{ref}/c_0 p_{ref}^2) - 20 \log F(St) \quad (11)$$

where ρ_0, Δf_{ref}, p_{ref}, and c_0 are density of air (1.21 kg/m^3), frequency increment of 1Hz, reference pressure of 20 μPa, and speed of sound, respectively. The sound pressure level of spectral density, L_{pp}, is obtained by the relation of $L_{pp} = 10 \log[S_{pp} \Delta f_{ref}/p_{ref}^2]$.

The frequency range is limited by the first cut-off frequency of the inlet duct, which is 1380Hz. After specifying the Strouhal number, the G function of different Helmholtz numbers is obtained by changing the rotational speed of fan, only with an unknown constant from the F function. Two consecutive Strouhal numbers of St and $St + \Delta St$ give an overlapping range of Helmholtz number:

$$(St + \Delta St)\left(\Omega_{min} - \frac{\Delta\Omega}{2}\right)\frac{Dn}{60c_0} \le He \le St\left(\Omega_{max} + \frac{\Delta\Omega}{2}\right)\frac{Dn}{60c_0} \quad (13)$$

where Ω is the rotational speed in rev./min. The offsets in level can be minimized numerically shifting each curve by a weighted average of differences in levels from all the other overlapping curves approximated by polynomials. To produce a smooth, continuous G function, the scattered data are filtered using the adjacent averaging method.

Figure 9 shows acoustic response functions determined by Mongeau et al.'s method and our weighted average method, which are almost identical with small deviations in low Helmholtz numbers. The resolution of the procedure can be improved by using a smaller increment of Strouhal number up to $\Delta St = 0.1$. The number of

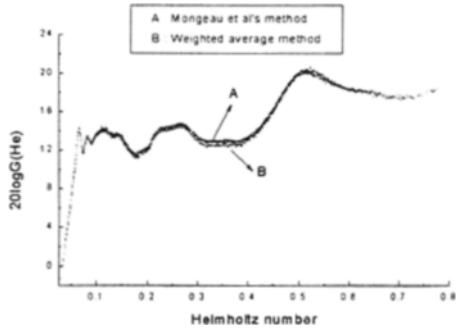

Fig. 9 Comparison of acoustic response function determined by two averaging methods for the case of $p_\theta = 1$.

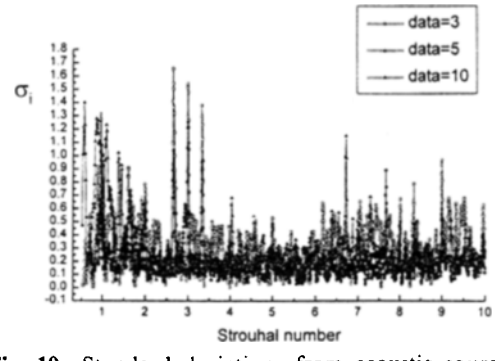

Fig. 10 Standard deviations from acoustic source spectra of $p_\theta = 1$ for three cases of rotational speeds.

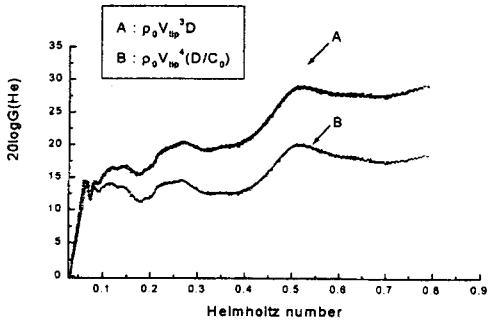

Fig. 11 Acoustic response functions by two different scaling parameters for the case of $p_\theta = 1$.

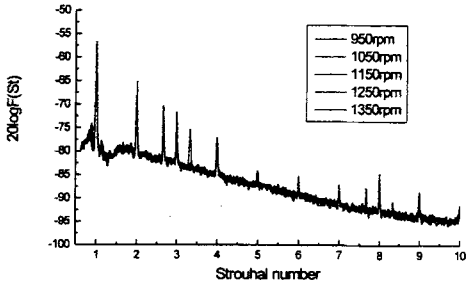

Fig. 12 The source spectral distribution function determined by the in-duct method for the case of $p_\theta = 1$.

rotational speeds also affect the standard derivations at each Strouhal number, as shown in Fig. 10, where the mean square errors are reproduced as an indication of accuracy for the spectral decomposition. Two different scaling parameters for low-frequent gust problems produce quite different acoustic behaviors in the G function as shown in Fig. 11. The case with a convective correlation time-scale is considered to include impedance effects in the G function, whereas the effect of impedance are put together with the scaling parameter for our case with an acoustic correlation time-scale.

The source spectral distribution function F can be obtained by substracting G(He) from their spectrum of L_{pp}. The results are given in Fig. 12 through Fig. 15 for four different non-uniform inlet conditions. From the fact that all five spectra collapse into a single curve within a few dB, it can be stated that the scaling parameters for the spectral energy density are effective at low Strouhal

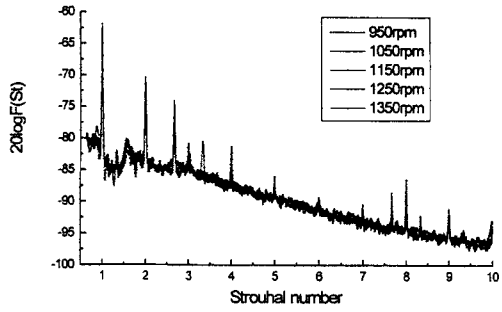

Fig. 13 The source spectral distribution function determined by the in-duct method for the case of $p_\theta = 2$.

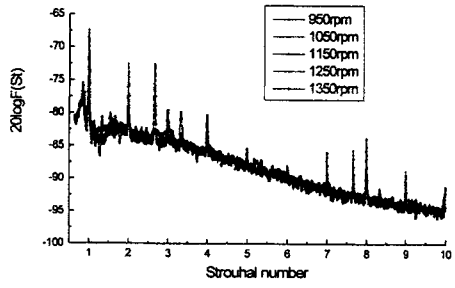

Fig. 14 The source spectral distribution function determined by the in-duct method for the case of $p_\theta = 4$.

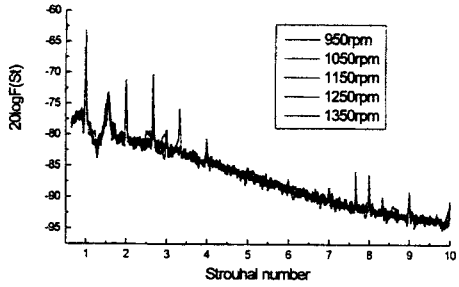

Fig. 15 The source spectral distribution function determined by the in-duct method for the case of $p_r = 1.5$.

numbers for the low-frequency inflow distortions.

The source spectral distribution functions from various non-uniformities show more prominent peaks at each Strouhal number than the normalized cross-spectra given in Fig. 8. The azimuthal disturbance of $p_\theta = 1$ introduces relatively more compact inflow distortion, where the blades go through the fluctuations of total loading as a whole, and generates an increased level of discrete

sound at the first a few BPFs, as shown in Fig. 12. The azimuthal disturbance of $p_\theta=4$ makes the blade to respond locally to the incoming turbulence and is radiated as scattered sounds of dipole-type source. The radial disturbance of $P_r=1.5$ develops the non-BPF rotating instability at a Strouhal number of 1.54, as shown in Fig. 15, which is also considered to radiate noise scattered at the trailing edges.

5. Conclusions

A method characterizing the noise sources, which is based on the spectral decomposition method, was successfully applied to study both compact and non-compact sound from non-uniform incoming flows of low-frequent gusts for the propeller-type axial fan. The acoustic pressures from the rotating blades, which encounter the low-frequent gusts, were used to identify the noise source spectra for the various non-uniform incoming flows. The azimuthal disturbance of $p_\theta=1$ introduced relatively compact inflow distortion and pronounced levels of about 20 dB at a few discrete BPF's. These scalings turned out to be effectively applied to investigate the relatively low-frequency noise generation mechanisms for the propeller-type axial fan with various non-uniform inlet conditions.

References

Atassi, H. M. and Dusey, M. P. 1990, "Acoustic Radiation from a Thin Airfoil in Nonuniform Subsonic Flows," *AIAA paper*, No. 90-3910

Madison, R. D., 1949, *Fan Engineering*, Fifth Edition, Buffalo Forge Company, U. S. A.

Weidemann, J. , 1971, "Analysis of the Relations between Acoustic and Aerodynamic Parameters for a Series of Dimensionally Similar Centrifugal Fan Rotors," *NASA-TT-F-13798*.

Neise W., 1975, "Application of Similarity Laws to the Blade Passage Sound of Centrifugal Fans," *J. Sound and Vib.*, Vol. 43(1), pp. 61~75.

Longhouse, R. E., 1976, "Noise Mechanism Separation and Design Considerations for Low Tip-Speed, Axial-flow Fans," *J. Sound and Vib.*, Vol. 48, pp. 461~474

Margetts, E. J., 1987, "A Demonstration that an Axial Fan in a Ducted Inlet Ducted Outlet Configuration Generates Predominantly Dipole Noise," *J. Sound and Vib.* Vol. 117(2), pp. 399~406

Mongeau, L., Thompson, D. E., and Mclaughlin, D. K., 1995, "A Method for Characterizing Aerodynamic Sound Sources in Turbomachines," *J. Sound and Vib.*, Vol. 181(3), pp. 369~389.

Goldstein, M. E., 1976, *Aeroacoustics*, McGraw-Hill Inc., New York.

Lighthill, M. J., 1952, "On Sound Generated Aerodynamically; I. General Theory," *Proc. Roy. Soc. London Ser.* A. 211, pp. 564~587.

Ffowcs Williams, J. E., Hawkings, D. L., 1969, "Theory Relating to the Noise of Rotating Machinery," *J. Sound and Vib.*, Vol. 10, No. 1, pp. 10~21.

Ffowcs Williams, J. E., Hall, L. H., 1970, "Aerodynamic Sound Generation by Turbulent Flow in the Vicinity of a Scattered Half Plane," *J. Fluid Mech.*, Vol. 40, No. 4, pp. 657~670.

International Standards Organization, 1990, ISO 5136 *Acoustics-Determination of Sound Power Radiated into a Duct by Fans-In-duct Method*.

ANSI/AMCA210-85, 1985, *American National Standard Laboratory Methods of Testing Fans for Rating*.

Krane, M. H., Bent, P. H., and Quinlan, D. A., 1995, "Rotating Instability Waves as a Noise Source in a Ducted Axial Fan," *NCA*-Vol. 21, 1995 IMECE, ASME, pp. 19~40.

Choi, J. -S., 1994, "Aerodynamic Noise Generation in Centrifugal Turbomachinery," *KSME Int'l J.*, Vol. 8, No. 2, pp. 161~174.

Neise W., Holste, F., Miranda, L., and Herrmann, M., 1995, "Free-field Sound Power Levels of Open-outlet Fans and Comparison with In-duct Measurements," *Noise Control Eng. J.*, Vol. 43(4), pp. 129~143.